

# miR-141-3p-loaded extracellular vesicles ameliorate intrahepatic bile duct stone disease by decreasing MUC5AC expression *via* the MAPK pathway

Yinbiao Cao, Shichun Lu\*, Haowen Tang\*

Faculty of Hepato-Pancreato-Biliary Surgery, Chinese PLA General Hospital, Beijing, China.

**SUMMARY:** Intrahepatic bile duct stone disease has a high morbidity in China, with a high rate of additional surgery, a high rate of cancer development, and a high disease burden. Activation of the MAPK pathway leading to up-regulation of MUC5AC expression is an important factor in the formation of intrahepatic bile duct stones. Exosomes or extracellular vesicles (EVs) can be used as therapeutic vectors to encapsulate and carry drugs into diseased cells to achieve a therapeutic effect. The current study alleviated intrahepatic bile duct stone disease by preparing EVs carrying miR-141-3p. First, the researchers loaded mesenchymal stem cell (ESC)-derived EVs with miR-141-3p (miR-141-3p-EVs) and verified the phenotypes and characteristics of miR-141-3p-EVs. miR-141-3p-EVs successfully reduced the inflammatory level of human biliary epithelial cells (HIBEC) and lowered, *via* the MAPK pathway, MUC5AC expression. In an experiment involving an animal model of intrahepatic bile duct stones, miR-141-3p-EVs effectively alleviated stone formation, and the intrinsic mechanism was associated with the decreased level of MAPK pathway expression. In conclusion, results suggested that the EV-based strategy of miR-141-3p delivery to intrahepatic bile duct epithelial cells has value and provides a new approach for the treatment of intrahepatic biliary stone disease.

**Keywords:** hepatolithiasis, extracellular vesicles, miR-141-3p, MAPK, MUC5AC

## 1. Introduction

Intrahepatic bile duct stones (hepatolithiasis, or HL) occur above the confluence of the left and right hepatic ducts and may simultaneously be associated with extrahepatic bile duct stones (1). The prevalence of HL accounts for approximately 0.6% to 21.2% of primary cholelithiasis cases (2). HL is characterized by a prolonged and recurrent course that is difficult to cure. In the late stages of the disease, complications such as biliary cirrhosis, portal hypertension, and diffuse hepatic parenchymal destruction may occur, with a high risk of malignant transformation into intrahepatic cholangiocarcinoma (ICC), an extremely malignant cancer. Current research suggests that in China, HL is a significant risk factor for ICC, with a relative risk of 5.765. Globally, approximately 2% to 10% of HL cases may develop into ICC (3-5). Currently, the primary treatment for HL relies on surgical intervention. However, the postoperative residual stone rate is high, with a frequent recurrence of stones, leading to a reoperation rate ranging from 37.1% to 74.4%. Additionally, surgical procedures often result in severe complications, contributing to high morbidity

and mortality rates. These factors present significant challenges in the clinical management of HL (6-10).

Bacteria and the infections they cause are significant contributors to the development of intrahepatic bile duct stones. Clinical studies have found that the bile of HL patients contains a large number of Gram-negative bacteria. Lipopolysaccharides (LPSes), which are one of their metabolic products, can stimulate biliary epithelial cells to activate cytokines and inflammatory mediators. This process leads to chronic proliferative inflammatory changes in the intrahepatic bile ducts, accompanied by the hypersecretion of mucin MUC5AC. This pathological change is considered a primary characteristic of HL (11,12). Previous studies have reported that miR-141-3p can negatively regulate the EGFR/ERK pathway, thereby inhibiting the progression of inflammation or tumors (13-15). Since LPS-induced overexpression of MUC5AC plays a critical role in the formation of intrahepatic bile duct stones, miR-141-3p may serve as a novel target for the prevention and treatment of this condition (16).

Small extracellular vesicles (sEVs) are bilayer membrane-like vesicles capable of carrying proteins, lncRNAs, miRNAs, and lipid components. The

protective nature of these vesicles prevents the degradation of these small molecules in the extracellular environment, allowing them to be taken up by recipient cells. Once inside the recipient cells, these molecules can regulate gene expression and protein synthesis, playing a crucial role in intercellular communication, surface modification, and other cellular functions (17-20). Exosomes derived from mesenchymal stem cells (dMSC-sEVs) are characterized by their safety and low level of immunogenicity, enabling the delivery of various small molecule drugs, chemotherapeutic agents, and RNA fragments. These exosomes have been utilized in several clinical trials and have yielded promising outcomes (21). Exosomes that enter the bloodstream circulate alongside red blood cells and are primarily taken up by the liver and spleen (22). Therefore, using exosomes as a delivery vehicle theoretically allows for the efficient targeting of liver tissues with effector molecules. In the current study, we prepared exosomes derived from mesenchymal stem cells loaded with miR-141-3p and applied them to human intrahepatic biliary epithelial cells (HIBECs) treated with LPS. We then assessed cell proliferation, migration capabilities, and the level of EGFR/ERK pathway expression to evaluate the effects of miR-141-3p-EVs and we further explored their potential mechanisms.

## 2. Materials and Methods

### 2.1. Cell culture

An HIBEC cell line was purchased from Otwo Biotech Company (Shen Zhen, China). HIBEC cells were cultured in RPMI-1640 medium (Gibco, USA) supplemented with 10% fetal bovine serum (FBS) (Gibco, USA) and a 1% penicillin-streptomycin solution (Gibco, USA). All cells were maintained in a 5% CO<sub>2</sub> atmosphere at 37 °C. The cells were subcultured when the confluence reached 80%. The current study used cells at passage 3. HIBEC cells were digested with 0.25% trypsin and resuspended in RPMI-1640 medium.

### 2.2. Isolation of EVs

Extracellular vesicles (dMSC-sEVs) were isolated and purified from the supernatant *via* ultracentrifugation. Initially, the MSC cell culture medium was centrifuged at 2,000 x g for 10 min to eliminate cell debris. The supernatant was then collected and centrifuged at 10,000 x g for 30 min. The new supernatant obtained underwent ultracentrifugation at 100,000 x g for 75 min. This supernatant was again collected and centrifuged at 10,000 x g for 30 min, followed by another ultracentrifugation of the new supernatant at 100,000 x g for 75 min. The resulting pellet was resuspended in 1 mL of PBS and filtered through a 0.22- $\mu$ m filter. This suspension was then subjected to a final ultracentrifugation at 100,000 x

g for 75 min. The dMSC-sEVs were resuspended in PBS and stored at -80 °C.

### 2.3. Preparation of miR-141-3p-loaded exosomes *via* electroporation

hsa-miR-141-3p (ID: MIMAT0000432) was purchased from GeneCopoeia. In a 60-mm dish containing 5 mL of exosome-free culture medium (with 50-70% cell confluence), 200 pmol of miR-141-3p or its inhibitor was mixed with 20  $\mu$ g of exosomes in PBS, followed by the addition of CaCl<sub>2</sub> to achieve a final concentration of 0.1 M. The final volume was adjusted to 300  $\mu$ L using sterile PBS. The mixture was then incubated on ice for 30 min. After heat shocking at 42°C for 60 seconds, the mixture was placed back on ice for an additional 5 min. For RNase treatment of exosomes, the exosomes were incubated with RNase (5  $\mu$ g/mL; EN0531, Thermo Fisher) at 37°C for 30 min. During electroporation, miR-141-3p was mixed with dMSC-sEVs at a 1:1 ratio (weight/weight) in electroporation buffer. The mixture was loaded into a Neon Tip and electroporated six times at 0.5 kV with 220-ms pulses, according to the manufacturer's instructions (Thermo Fisher Scientific).

### 2.4. Characteristics of EVs and MIR-141-3P-EVs

The size and concentration of EVs and miR-141-3p-EVs were measured using Nanoparticle Tracking Analysis (NTA) (Particle Metrix GmbH, Germany), and their morphology was observed using transmission electron microscopy (TEM).

### 2.5. Labeling of EVs

The membrane of HIBECs were labeled with PKH67 (green) and DAPI (cell nucleus, blue). EVs were counterstained with actin (cytoskeleton, red). Images were captured using a confocal microscope (Leica, Germany).

### 2.6. Cell proliferation

HIBEC cells ( $5 \times 10^3$  cells per well) were seeded into 96-well plates (Corning Inc, USA) and subjected to treatment with PBS, LPS (100  $\mu$ g/mL), EVs ( $2 \times 10^{10}$  particles/mL), and miR-141-3p-EVs ( $2 \times 10^{10}$  particles/mL) for 24, 48, and 72 h. Optical density (OD) values were recorded at a wavelength of 450 nm using an automated plate reader. Cell proliferation was evaluated using the BeyoClick™ EdU Cell Proliferation Kit. After the cells were fixed with 4% paraformaldehyde and permeabilized with 0.3% Triton X-100 (Beyotime, China), they were sequentially incubated in the Click reaction mixture and Hoechst 33342 at room temperature, followed by imaging under a fluorescence microscope.

## 2.7. HIBEC cell migration assay

The migratory characteristics of HIBECs were evaluated using transwell and scratch assays. For the transwell assay, HIBECs were suspended in serum-free medium at a density of  $5 \times 10^3$  cells/mL, and 100  $\mu$ L of the cell suspension was seeded into the upper chamber of a 24-well plate with an 8.0- $\mu$ m polycarbonate membrane (Corning Inc, USA). Different media were then added to the lower chamber. After the cells were cultured at 37°C with 5% CO<sub>2</sub> for 24 h, migrating cells were stained with 0.1% crystal violet for 7 min. Finally, stained cells were observed under an optical microscope, and images were captured.

For the scratch assay, HIBECs were seeded into a 6-well plate. Once the cells reached 90% confluence, a pipette tip was used to scratch the cell layer. Images of the cells were captured using a microscope at 0 and 24 h post-scratch. The number of migrating cells and the distance between the two boundaries of the scratch were calculated using the software ImageJ. The migration rate was calculated as follows: Cell migration rate = (1 - width of the gap area (at 12 or 24 h) / width of the gap area (at 0 h))  $\times$  100%.

## 2.8. Real-time reverse transcription polymerase chain reaction (RT-qPCR)

Total RNA was isolated from the miR-141-3p solution using the TRIzol<sup>®</sup> LS reagent (Invitrogen, Waltham, MA, USA). The quantity and quality of RNA samples were assessed using a Nanodrop 2000 (Thermo Fisher Scientific, San Jose, CA, USA) and RNA denaturing agarose gel electrophoresis. Complementary DNA (cDNA) was synthesized from RNA samples (OD260/280 ratio: 1.8-2.1; 28S/18S ratio: 2.0-2.5) using oligo (dT) and random primers (Thermo Fisher Scientific) and the Omniscript RT kit (Qiagen, Hilden, Germany). The RNA samples were further verified using RNA denaturing agarose gel electrophoresis. RNA expression was analyzed using the SYBR Premix Ex Taq<sup>™</sup> II kit (Takara, Kusatsu, Japan), with cDNA prepared at a 1/4 dilution. The internal control primer HsnRNA U6 and the target primer hsa-miR-141-3p were purchased from GeneCopoeia. Standard curves were generated for each primer pair, and amplification efficiency was calculated using the formula  $E = 10^{(-1/\text{slope})}$ . Relative levels of RNA expression were calculated using the  $2^{-\Delta\Delta C_t}$  method based on the threshold cycle (C<sub>t</sub>) values.

## 2.9. Western blotting

Proteins extracted using RIPA buffer were separated using SDS-polyacrylamide gel electrophoresis (SDS-PAGE) and then electrotransferred onto a polyvinylidene fluoride (PVDF) membrane. The membrane was

incubated with 5% non-fat milk for 1 h and then incubated overnight at 4°C with primary antibodies. These primary antibodies included anti-p-EGFR (1:1000, Abcam, USA), anti-GADPH (1:1000, Abcam, USA), anti-p-RAS (1:1000, Abcam, USA), anti-p38 (1:1000, Abcam, USA), anti-ERK-1 (1:1000, Abcam, USA), anti-MUC5AC (1:1000, Abcam, USA), and anti-p-ERK-1 (1:1000, Abcam, USA). After the membrane was washed, it was incubated with horseradish peroxidase (HRP)-conjugated secondary antibody (1:3000, ZSGB-BIO, China) at room temperature for 1 h. Antibody reactivity was detected using an ECL kit (Solarbio, China), and imaging was performed with the UVITEC Alliance MINI HD9 system (UVITEC, UK). The grayscale values representing levels of protein expression were quantified using the software ImageJ.

## 2.10. Creation of a mouse model of intrahepatic bile duct stone disease and treatment with miR-141-3p

All research plans and procedures were approved by the Institutional Animal Care and Use Committee. Male SD rats (BKS-Dock Leprem2Cd479, DB/db), aged 8 weeks, were purchased from SPF (Beijing, China) Biotechnology Co., Ltd. and were housed under standard laboratory animal conditions. Bile duct stone surgery was performed in the rat model as follows: a) The abdominal cavity was accessed by making a midline incision and gradually entering the peritoneal cavity layer by layer. b) The distal end of the common bile duct was isolated and silk suture was looped around it in preparation for ligation. c) The distal end of the common bile duct was ligated. d) Five 5 min were allowed to pass for the common bile duct above the ligation point to fill. e) A second ligature was placed above the first ligation point and a 24G cannula needle was used to puncture the common bile duct. After the rigid needle core was removed, the flexible needle was further advanced into the bile duct while ensuring that the second ligature remained within range of the needle body. f) The second ligature was tightened to secure the puncture needle. g) Point-two-five mg/mL of an LPS solution was injected at a dose of 0.5 mg/kg body weight. h) After the injection, the flexible needle was removed and the puncture site was ligated twice above the insertion point. i) The common bile duct was severed between the two ligatures placed in step (h) to induce bile duct obstruction. A total of 15 rats were randomly divided into three groups, with each group receiving different treatments *via* tail vein injection: a) PBS, b) dMSC-sEVs, and c) dMSC-sEVs-miR-141-3p. These treatments were administered to assess the therapeutic effects of dMSC-sEVs-miR-141-3p *in vivo*.

One week after induction of bile duct stones, bile samples were collected *via* common bile duct cannulation. The samples were centrifuged at 12,000 r/min for 10 min to remove the supernatant, and the

sediment was prepared for smearing. The experiment was conducted at a controlled room temperature of 25-30°C. The bile characteristics were observed using an Olympus microscope (polarized light). Additionally, the common bile duct, along with portions of the hepatic bile ducts and liver tissue, were excised for immunohistochemical analysis.

2.11. Histological analysis

Tissues from the bile duct were fixed in 4% paraformaldehyde, gradually dehydrated, and then embedded in paraffin. Five μm-thick sections of the embedded tissue were stained using the Hematoxylin and Eosin (H&E) Staining Kit (Solarbio, China) and Masson's Trichrome Staining Kit (Solarbio, China). For immunohistochemical staining, the sections, following deparaffinization, hydration, and antigen retrieval, were incubated overnight at 4 °C with primary antibodies anti-p-EGFR (1:1000, Abcam, USA), anti-GADPH (1:1000, Abcam, USA), anti-p-RAS (1:1000, Abcam, USA), anti-p38 (1:1000, Abcam, USA), anti-p-ERK-1 (1:1000, Abcam, USA), and anti-MUC5AC (1:1000, Abcam, USA). For immunohistochemistry, the sections were incubated with HRP-conjugated secondary antibody (1:200, Abcam, USA) at room temperature for 1 h. Immunocomplexes were visualized using the DAB Kit (ZSGBBIO, China). Images were recorded under a microscope and analyzed using the software Image-Proplus 6.0.

2.12. Statistical analysis

All data are expressed as the mean ± standard deviation. Comparisons between two groups were done using the

unpaired Student's *t*-test, while comparisons among multiple groups were done using one-way ANOVA. A difference was considered statistically significant when *p* < 0.05.

3. Results

3.1 Preparation and characterization of EVs and miR-141-3p-EVs

EVs were isolated from the culture medium of mesenchymal stem cells. miR-141-3p was then incubated at 37°C and incorporated into the EVs using electroporation. Free miR-141-3p was removed by ultracentrifugation, and purified miR-141-3p-EVs were obtained by resuspending the pellet. TEM revealed that the EVs exhibited the characteristic cup-shaped and smooth bilayer structure, and they retained their original morphology after miR-141-3p incorporation (Figure 1A). Nanoparticle tracking analysis (NTA) indicated that the initial EVs had a diameter of 115.2 ± 1.7 nm, which increased to 136 ± 1.4 nm after miR-141-3p incorporation. In the saline control group, the median diameter of EVs was 141.6 ± 10 nm (Figure 1B). These changes in morphology and particle size are likely due to the encapsulation of miR-141-3p, as well as the incubation at 37°C and repeated ultracentrifugation steps. qPCR analysis of the miR-141-3p-EVs indicated a significantly higher level of miR-141-3p expression in the miR-141-3p-EVs compared to that in the NC-EVs group (Figure 1C). These findings confirm that the miR-141-3p-EVs meet the characterization standards for extracellular vesicles, consistent with their potential as a next-generation drug delivery platform. Uptake experiments demonstrated that, after 12 h, EVs from both

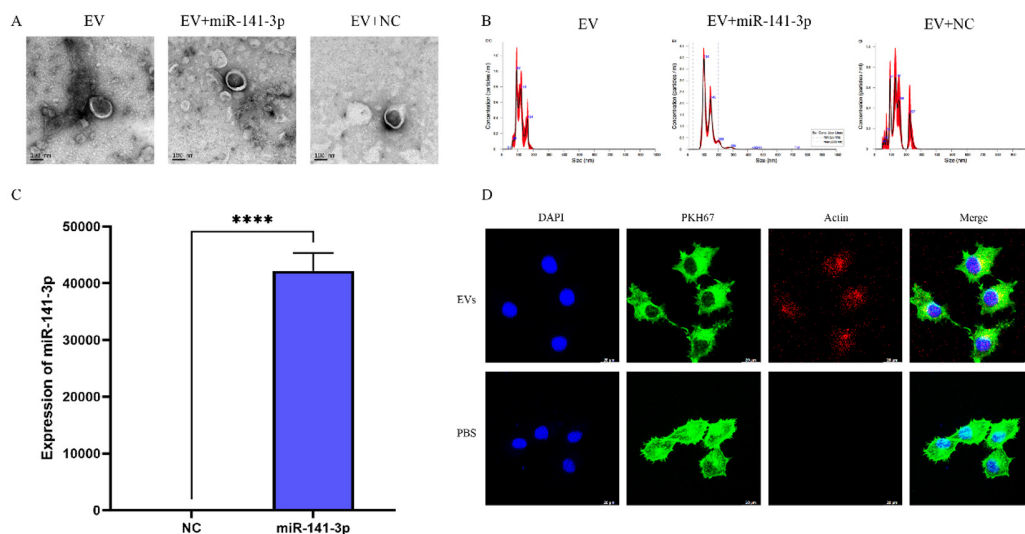


**Figure 1. Preparation and characterization of EVs and miR-141-3p-EVs.** (A) TEM images showing the morphology of EVs, EV-miR-141-3p, and EV-NC. (B) NTA results indicating the particle size distribution of exosomes in different groups. (C) Levels of miR-141-3p expression in miR-141-3p-EVs. (D) Exosome uptake assay: EV membranes were labeled with actin (red), HIBEC cell membranes were labeled with PKH67 (green), and nuclei were labeled with DAPI (blue).

groups (PKH26, red fluorescence) were successfully transferred into HIBECs (HIBEC cell membranes labeled with PKH67, green fluorescence; nuclei labeled with DAPI). As shown in Figure 1D, there was no difference in the uptake rates of the two groups, suggesting that the observed differences in biological function are due to the different compounds encapsulated within the vesicles.

### 3.2. miR-141-3p-EVs downregulate MUC5AC expression and inhibit intrahepatic bile duct stone formation

The proliferative capacity of HIBEC cells under different treatment conditions was assessed using the EdU assay (Figure 2). Green fluorescence indicates proliferating HIBEC cells. LPS was the most potent promoter of cell proliferation, while HIBEC cells treated with miR-141-3p-EVs displayed a significant reduction in proliferation compared to the group treated with exosome analogs (Figure 2, A and B). The migratory ability of HIBEC cells under different culture conditions was evaluated using a scratch assay. Scratch assays were performed 24 h after treatment with PBS, LPS, EVs, or miR-141-

3p-EVs. HIBEC cells treated with miR-141-3p-EVs exhibited a significantly lower scratch closure rate after 24 h compared to other groups (Figure 2, C and D). A transwell assay further indicated that the LPS group had the largest migration area of HIBEC cells while those treated with miR-141-3p-EVs had the smallest migration area, and it differed significantly compared to that in the LPS group (Figure 2, E and F).

### 3.3. miR-141-3p-EVs regulate MUC5AC expression via the MAPK pathway

Western blotting indicated that the expression of MAPK pathway proteins was consistently downregulated in HIBEC cells treated with AG1478, and miR-141-3p-EVs demonstrated more potent ability to downregulate MUC5AC gene expression in HIBEC cells (Figure 3A). In contrast, the levels of MAPK and MUC5AC protein expression in HIBEC cells treated with EVs or miR-141-3p-EV inhibitors did not decrease significantly. This experiment confirmed that miR-141-3p-EVs inhibit the formation of intrahepatic bile duct stones by downregulating the MAPK pathway and reducing levels

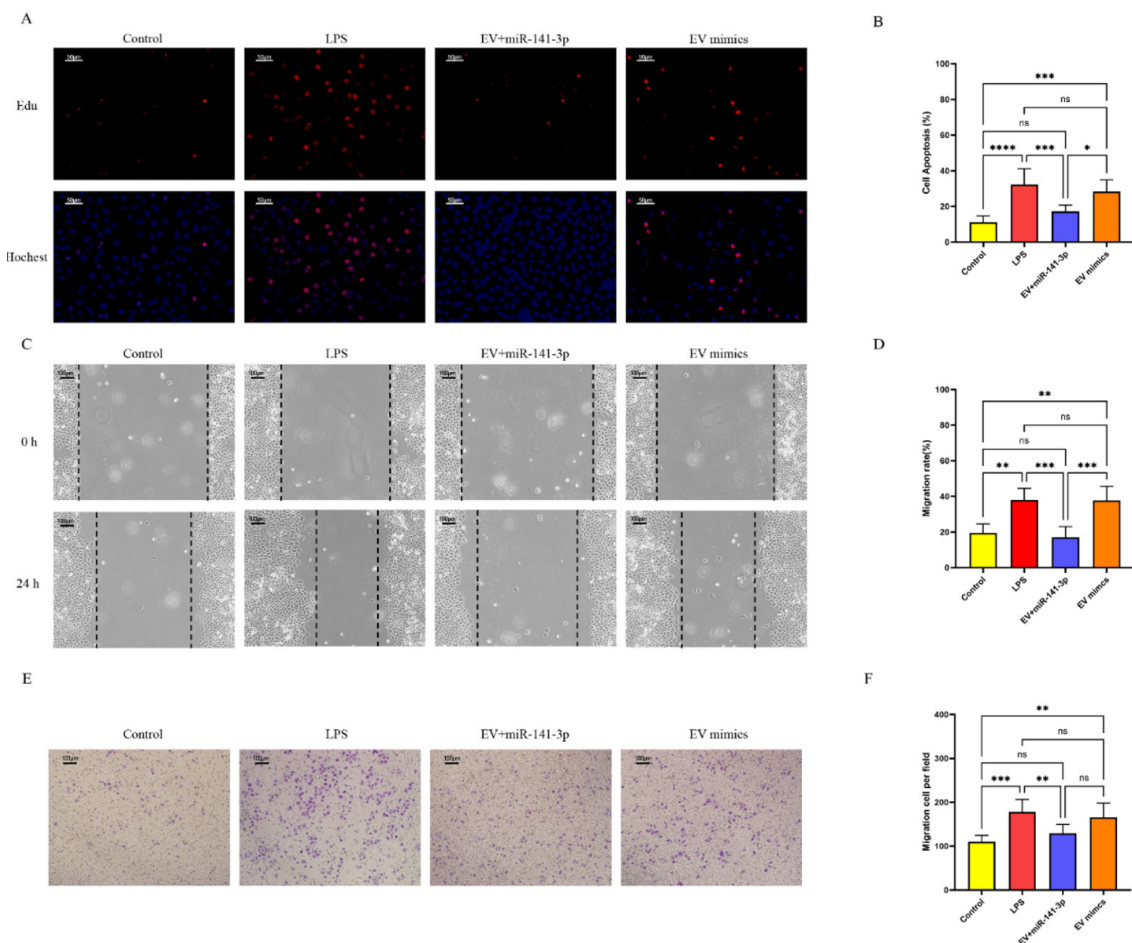


**Figure 2. miR-141-3p-EVs inhibit an LPS-induced inflammatory response and proliferation in HIBECs.** (A) EdU assay (EdU-positive cells are labeled green, and nuclei in each group are labeled in red). (B) Quantification of the rate of EdU-positive cell proliferation ( $n = 7$ ). (C) Scratch assay (images taken at 0h and 24h post-scratch). (D) Statistical analysis of the scratch closure area ( $n = 7$ ). (E) Representative images of the transwell assay of HIBECs in different groups. (F) Quantitative analysis of HIBEC migration in the transwell assay.

of MUC5AC expression.

### 3.4. Effect of miR-141-3p-EVs on intrahepatic bile duct stone formation in rats

In animal experiments (Figure 4), dMSC-sEVs-miR-141-3p had a positive therapeutic effect on rats with induced intrahepatic bile duct stones. Observations of rat bile under polarized light microscopy revealed that the bile in the dMSC-sEVs-miR-141-3p group was noticeably thinner, with significantly fewer bile stones formed compared to those in the control group.

In the immunohistochemical experiment (Figure 5), the bile duct tissue of rats in the dMSC-sEVs-miR-141-3p group displayed significantly lower levels of EGFR, p-ERK, RAS, and MUC5AC expression compared to those in the LPS group and the LPS+EV+EV inhibitor group. These decreases were significant.

## 4. Discussion

This study successfully prepared exosomes loaded with miR-141-3p and validated their stable and reliable drug delivery properties. Findings indicated that miR-141-3p-EVs can reduce LPS-induced inflammatory responses in intrahepatic biliary epithelial cells and, to some extent, inhibit the formation of intrahepatic bile duct stones. *In vitro* studies demonstrated that LPS promotes inflammatory responses in HIBECs while miR-141-3p-EVs alleviate these LPS-induced inflammatory responses by downregulating the MAPK pathway. *In vivo* experiments confirmed that intravenous administration of miR-141-3p-EVs effectively reduces bile duct stone

formation and decreases the level of MAPK pathway expression in biliary epithelial cells.

Previous studies have confirmed that LPS induces the overexpression and secretion of MUC5AC *via* the EGFR/ERK pathway. The polymerized form of MUC5AC, along with its abundant O-linked oligosaccharides, increases bile viscosity, thereby accelerating stone formation. Additionally, MUC5AC can constitute a major component of bile duct stones, aggregating bile constituents such as bilirubin crystals and desquamated epithelial cells to form the core and scaffold of calcium bilirubinate stones (23,24). Therefore, targeting the EGFR/ERK pathway-mediated overexpression of MUC5AC may inhibit this pathway, preventing stone formation and recurrence, and it could effectively reduce the incidence of intrahepatic bile duct stones. This study developed mesenchymal stem cell-derived exosomes loaded with miR-141-3p. Experiments demonstrated that miR-141-3p effectively downregulates the expression of the EGFR/ERK pathway and MUC5AC, leading to a reduction in the formation of intrahepatic bile duct stones.

MicroRNAs (miRNAs) are a class of endogenous small RNAs, approximately 20-24 nucleotides in length, which play critical regulatory roles in disease processes. Each miRNA can target multiple genes, and several miRNAs can regulate the same gene. Previous studies have shown that miR-141-3p can negatively regulate the EGFR/ERK pathway, thereby inhibiting the progression of inflammation or tumors. For instance, Xing *et al.* found that miR-141-3p suppresses the proliferation, migration, and invasion of colorectal cancer cells by downregulating the EGFR/ERK pathway

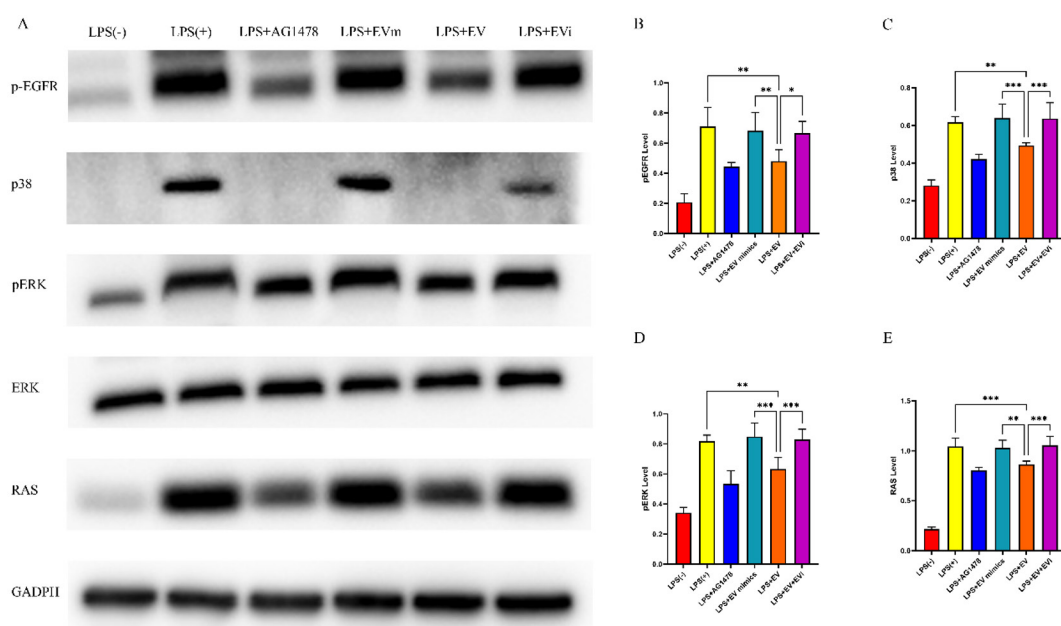


**Figure 3.** (A) Representative Western blotting images showing the expression of EGFR, p38, p-ERK1, RAS, and GAPDH in HIBECs under different treatment conditions: PBS, LPS, LPS + AG1478, LPS + EV mimics, LPS + EV, and LPS + EV + EVi. (B-E) Relative protein levels in each group, with p-EGFR, p38, and RAS normalized to GAPDH and p-ERK normalized to ERK.

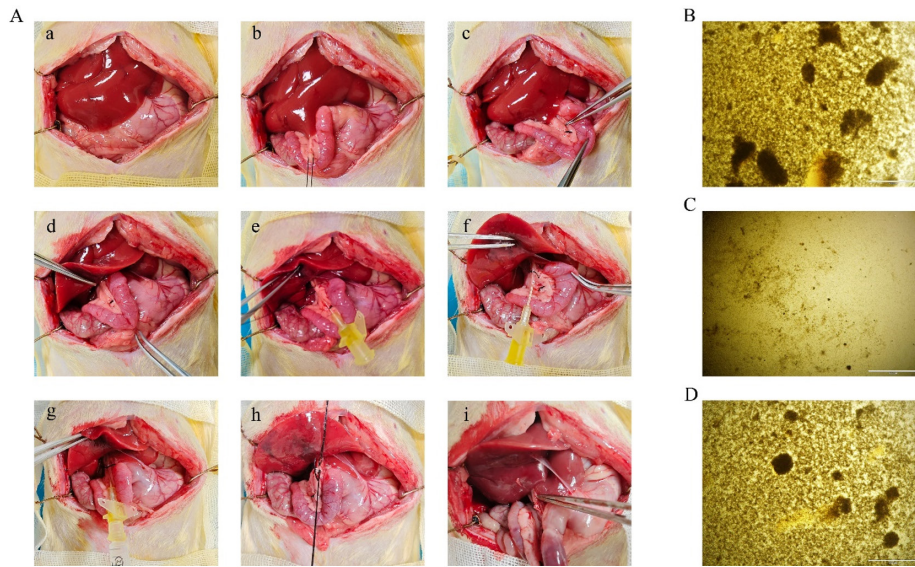


**Figure 4. Bile duct stone surgery in a rat model and bile microscopy from different groups.** (A) Images of bile duct stone surgery in a rat model: (a): Midline abdominal incision to access the abdominal cavity. (b): Isolation of the common bile duct with silk suture looped around it for marking. (c): Ligation of the distal end of the common bile duct. (d): Visible bile duct obstruction and dilation above the ligation point. (e): Placement of a pre-ligation suture and insertion of a 24G cannula needle above the ligation point. (f): Tightening of the pre-ligation suture to secure the cannula needle, with bile leakage indicating successful puncture. (g): Connection of a syringe and injection of 0.25 mg/mL LPS solution. (h): Removal of the cannula needle and ligation of the common bile duct above the puncture site. (i): Severing of the ligated common bile duct, resulting in obstruction and dilation above the ligation site. (B) Bile characteristics in rats injected with saline *via* the tail vein. (C) Bile characteristics in rats injected with dMSC-sEVs-miR-141-3p *via* the tail vein. (D) Bile characteristics in rats injected with dMSC-sEVs-miR *via* the tail vein.

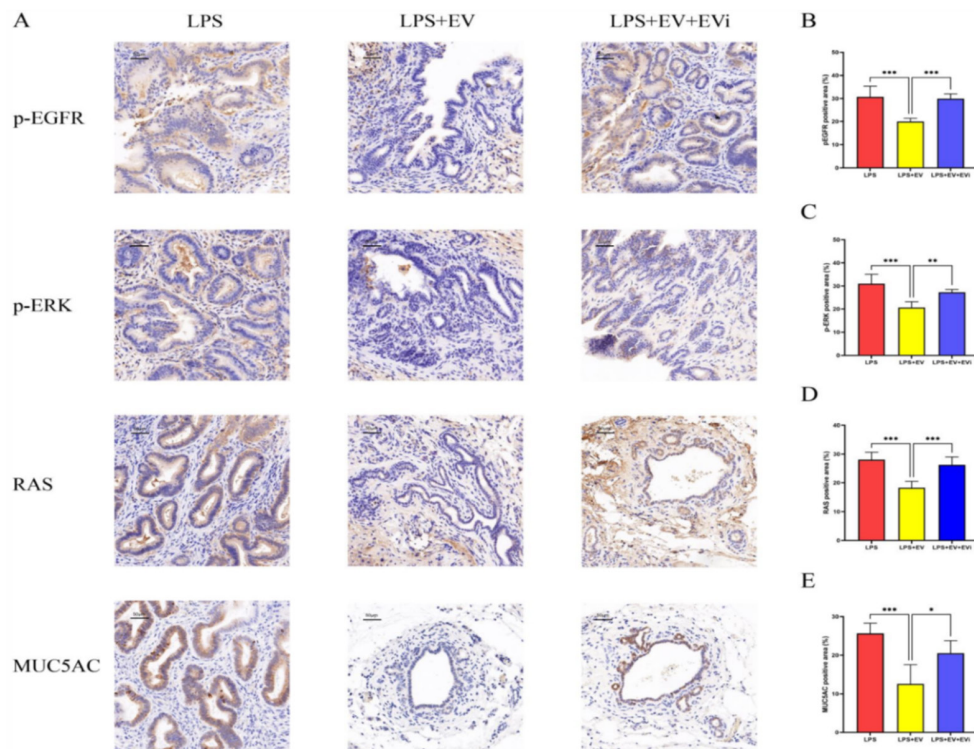


**Figure 5. Immunohistochemical results in rat bile duct tissue.** (A) Immunohistochemical staining of rat bile duct tissue. (B) Percentage of p-EGFR-positive areas. (C) Percentage of p-ERK-positive areas. (D) Percentage of RAS-positive areas. (E) Percentage of MUC5AC-positive areas.

(13). Similarly, Xue *et al.* reported that the bioceramic sealer iRoot SP promotes osteogenic differentiation of hSCAPs by inhibiting miR-141-3p, downregulating SPAG9 expression, and activating the MAPK pathway (25). Additionally, the antagonistic effects of miR-141-3p against LPS have also been increasingly explored. Xia *et al.* reported that miR-141-3p can counteract LPS-induced apoptosis and inflammatory responses in human lung fibroblasts (14). Similarly, Zhu *et al.* found that miR-141-3p can inhibit apoptosis and the expression of MUC5AC in LPS-pretreated nasal mucosal cells (15). As previously discussed, LPS-induced overexpression of MUC5AC plays a critical role in the formation of intrahepatic bile duct stones. Therefore, we hypothesize that miR-141-3p could be a novel target for the prevention and treatment of intrahepatic bile duct stones by downregulating MUC5AC expression via the EGFR/ERK pathway. Western blotting revealed that the expression of the EGFR/ERK pathway and MUC5AC in HIBEC cells stimulated with LPS increased significantly compared to that in the PBS group, and this is consistent with the mechanism by which LPS induces intrahepatic bile duct stone formation. However, exosomes loaded with miR-141-3p effectively reduced the expression of EGFR, ERK, RAS, and MUC5AC. In contrast, no negative regulation of the EGFR/ERK pathway was observed in groups treated with either exosomes alone or exosome inhibitors, suggesting that the downregulation of MUC5AC expression was mediated by miR-141-3p. A transwell assay indicated that miR-141-3p-EVs significantly reduced the migratory ability of LPS-treated HIBEC cells, further indicating that miR-141-3p lowers the inflammatory response in HIBEC cells. Similar results were observed in the scratch assay, where miR-141-3p-EVs reduced cell migration. Additionally, an EdU assay showed that HIBEC cells treated with miR-141-3p-EVs exhibited decreased proliferation compared to LPS-treated HIBEC cells. Since the EGFR/ERK pathway is closely associated with cell proliferation, the negative regulation of EGFR expression by miR-141-3p likely led to the observed suppression of HIBEC cell proliferation. These findings further confirm the effectiveness of miR-141-3p-EVs in negatively regulating EGFR expression.

In this study, Sprague-Dawley (SD) rats were used as experimental animals to establish an intrahepatic bile duct stone model. Based on research by Chang *et al.*, LPS was injected into the bile ducts to induce the formation of intrahepatic bile duct stones in the rabbits (26). The model was successfully created based on the characteristics of bile and stone morphology observed under a microscope. In the animal experiments, the bile duct tissues of rats injected with miR-141-3p-EVs exhibited significantly lower expression of EGFR, ERK, and MUC5AC proteins in immunohistochemical analyses, whereas rats injected with EV mimics showed minimal downregulation of EGFR, ERK, and MUC5AC expression. This result was further validated

by immunohistochemical findings in rat bile duct tissues, where intravenous injection of miR-141-3p-EVs notably reduced the expression of the MAPK pathway in the intrahepatic bile ducts and effectively decreased MUC5AC secretion, thereby inhibiting the formation of intrahepatic bile duct stones. Based on both *in vivo* and *in vitro* experiments, we conclude that EVs loaded with miR-141-3p can effectively reduce the expression of the EGFR/ERK pathway and further decrease MUC5AC secretion, achieving a therapeutic effect against intrahepatic bile duct stones.

We developed miR-141-3p-loaded exosomes as a novel therapeutic approach for treating intrahepatic bile duct stone disease. Exosomes are naturally produced by cells and are small vesicles that are highly biocompatible with the human body and have a low level of immunogenicity, making them less likely to trigger a strong immune response. MicroRNAs are prone to degradation in natural environments, but exosomes can stably carry RNA and other macromolecular drugs, protecting them from degradation by enzymes both outside and inside the body. Due to their targeting ability and low level of immunogenicity, RNA drugs delivered via exosomes may cause fewer adverse reactions than traditional delivery methods. In this study, use of exosomes as a delivery vehicle for miR-141-3p provided a safer, more effective, and targeted method of treatment, offering new insights into the development of novel drugs for the treatment of intrahepatic bile duct stone disease.

However, this study did have a limitation. The reduction of MAPK pathway activity in human tissues by miR-141-3p was not observed or investigated. Further studies are needed to explore the efficacy and safety of miR-141-3p-loaded exosomes in the treatment of intrahepatic bile duct stone disease.

In conclusion, we developed an exosomal drug harboring miR-141-3p, which alleviates intrahepatic bile duct stone disease by inhibiting the expression of the EGFR pathway in intrahepatic bile duct epithelial cells. It also demonstrated preliminary therapeutic effects for intrahepatic bile duct stone disease and has the potential to become a clinical therapeutic drug.

**Funding:** This work was supported by grants from the Beijing Natural Science Foundation (L244027), Beijing Natural Science Foundation (7234388) and Youth Independent Innovation Science Fund of PLAGH (22QNFC013).

**Conflict of Interest:** The authors have no conflicts of interest to disclose.

## References

1. Fujita N, Yasuda I, Endo I, *et al.* Evidence-based clinical practice guidelines for cholelithiasis 2021. *J Gastroenterol.*

- 2023; 58:801-833.
2. Wang P, Sun B, Huang B, Xie J, Liu Y, Zhu C, Ye C, Zhou Z. Comparison between percutaneous transhepatic rigid cholangioscopic lithotripsy and conventional percutaneous transhepatic cholangioscopic surgery for hepatolithiasis treatment. *Surg Laparosc Endosc Percutan Tech.* 2016; 26:54-59.
  3. Chen G, Yu H, Wang Y, Li C, Zhou M, Yu Z, Zheng X, Wu X, Shan Y, Zhang Q, Zeng Q. A novel nomogram for the prediction of intrahepatic cholangiocarcinoma in patients with intrahepatic lithiasis complicated by imagiologically diagnosed mass. *Cancer Manag Res.* 2018; 10:847-856.
  4. Xie GX, Shi FX, Li YC, Chen ZH, Li ML, Zhao J, Liu P, Xiang MQ, Guo W, Hu Q, Liu XY, Li HL. Analysis of clinicopathological features of intrahepatic bile duct stones and its related occult cholangiocarcinoma. *Zhonghua Bing Li Xue Za Zhi.* 2021; 50:388-390. (in Chinese)
  5. Moris D, Palta M, Kim C, Allen PJ, Morse MA, Lidsky ME. Advances in the treatment of intrahepatic cholangiocarcinoma: An overview of the current and future therapeutic landscape for clinicians. *CA Cancer J Clin.* 2023; 73:198-222.
  6. Kim HJ, Kang TU, Swan H, Kang MJ, Kim N, Ahn HS, Park SM. Incidence and prognosis of subsequent cholangiocarcinoma in patients with hepatic resection for bile duct stones. *Dig Dis Sci.* 2018; 63:3465-3473.
  7. Chinese Research Hospital Association, Society for Hepato-pancreato-biliary Surgery, Expert Committee of Public Welfare Scientific Research Program of National Health Commission. Guidelines for minimally invasive surgery for hepatolithiasis (2019 edition). *Chin J Gastrointest Surg.* 2019; 18:407-413. (in Chinese)
  8. Chinese Research Hospital Association, Society for Hepato-pancreato-biliary Surgery. Guideline for application of percutaneous transhepatic choledochoscopic lithotripsy in hepatolithiasis (2021 edition). *Chin J Hepatobil Surg.* 2022; 28:7-14. (in Chinese)
  9. Li C, Wen T. Surgical management of hepatolithiasis: A minireview. *Intractable Rare Dis Res.* 2017 May; 6(2):102-105.
  10. Li WN, Xiong YF, Zhu JJ, Yang G, Sun Y, Li JD. The difficulties and surgical decision analysis of laparoscopic technique in treating complicated hepatolithiasis. *Chin J Surg.* 2021; 59:279-283. (in Chinese)
  11. Zen Y, Harada K, Sasaki M, Tsuneyama K, Katayanagi K, Yamamoto Y, Nakanuma Y. Lipopolysaccharide induces overexpression of MUC2 and MUC5AC in cultured biliary epithelial cells: Possible key phenomenon of hepatolithiasis. *Am J Pathol.* 2002; 161:1475-1484.
  12. Wu X, Yao C, Kong J, Tian Y, Fan Y, Zhang Z, Han J, Wu S. Molecular mechanism underlying miR-130b-Sp1 transcriptional regulation in LPS-induced upregulation of MUC5AC in the bile duct epithelium. *Mol Med Rep.* 2021; 23:106.
  13. Xing Y, Jing H, Zhang Y, Suo J, Qian M. MicroRNA-141-3p affected proliferation, chemosensitivity, migration and invasion of colorectal cancer cells by targeting EGFR. *Int J Biochem Cell Biol.* 2020; 118:105643.
  14. Xia L, Zhu G, Huang H, He Y, Liu X. LncRNA small nucleolar RNA host gene 16 (SNHG16) silencing protects lipopolysaccharide (LPS)-induced cell injury in human lung fibroblasts WI-38 through acting as miR-141-3p sponge. *Biosci Biotechnol Biochem.* 2021; 85:1077-1087.
  15. Zhu YM, Wu F, Zhou JY. Analysis the effect of miR-141-3p/HMGB1 in LPS-induced mucus production and the apoptosis in nasal epithelial cells. *Kaohsiung J Med Sci.* 2020; 36:622-629.
  16. Liu Z, Tian F, Feng X, He Y, Jiang P, Li J, Guo F, Zhao X, Chang H, Wang S. LPS increases MUC5AC by TACE/TGF- $\alpha$ /EGFR pathway in human intrahepatic biliary epithelial cell. *Biomed Res Int.* 2013; 2013:165715.
  17. Babaei M, Rezaie J. Application of stem cell-derived exosomes in ischemic diseases: Opportunity and limitations. *J Transl Med.* 2021; 19:196.
  18. Ferguson SW, Wang J, Lee CJ, Liu M, Neelamegham S, Canty JM, Nguyen J. The microRNA regulatory landscape of MSC-derived exosomes: A systems view. *Sci Rep.* 2018; 8:1419.
  19. Chavez-Munoz C, Kilani RT, Ghahary A. Profile of exosomes related proteins released by differentiated and undifferentiated human keratinocytes. *J Cell Physiol.* 2009; 221:221-231.
  20. Xiao X, Xu M, Yu H, Wang L, Li X, Rak J, Wang S, Zhao RC. Mesenchymal stem cell-derived small extracellular vesicles mitigate oxidative stress-induced senescence in endothelial cells *via* regulation of miR-146a/Src. *Signal Transduct Target Ther.* 2021; 6:354.
  21. Li Q, Hu W, Huang Q, *et al.* MiR146a-loaded engineered exosomes released from silk fibroin patch promote diabetic wound healing by targeting IRAK1. *Signal Transduct Target Ther.* 2023; 8:62.
  22. Nong J, Glassman PM, Muzykantov VR. Targeting vascular inflammation through emerging methods and drug carriers. *Adv Drug Deliv Rev.* 2022; 184:114180.
  23. Yamasaki T, Nakayama F, Tamura S, Endo M. Characterization of mucin in the hepatic bile of patients with intrahepatic pigment stones. *J Gastroenterol Hepatol.* 1992; 7:36-41.
  24. Sasaki M, Nakanuma Y, Kim YS. Expression of apomucins in the intrahepatic biliary tree in hepatolithiasis differs from that in normal liver and extrahepatic biliary obstruction. *Hepatology.* 1998; 27:54-61.
  25. Xue K, Hu G, Wu L, Han H, Sun Y, Gan K, Zhu J, Du T. The bioceramic sealer iRoot SP promotes osteogenic differentiation of human stem cells from apical papilla *via* miR-141-3p/SPAG9/MAPK signalling pathway. *Int Endod J.* 2023; 56:1241-1253.
  26. Chang WH. A dynamic study on myoelectric waves and ultrastructure of oddi's sphincter during formation of primary intrahepatic stone in rabbits. *Third Military Medical University.* 2009. (in Chinese)
- Received September 5, 2024; Revised November 15, 2024; Accepted November 20, 2024.
- \*Address correspondence to:*  
Haowen Tang and Shichun Lu, Faculty of Hepato-Pancreato-Biliary Surgery, Chinese PLA General Hospital, 28 Fuxing Road, Haidian, Beijing, China 100853.  
E-mail: haowen\_tang@163.com (HT), lusc\_plagh@163.com (SL)
- Released online in J-STAGE as advance publication November 23, 2024.